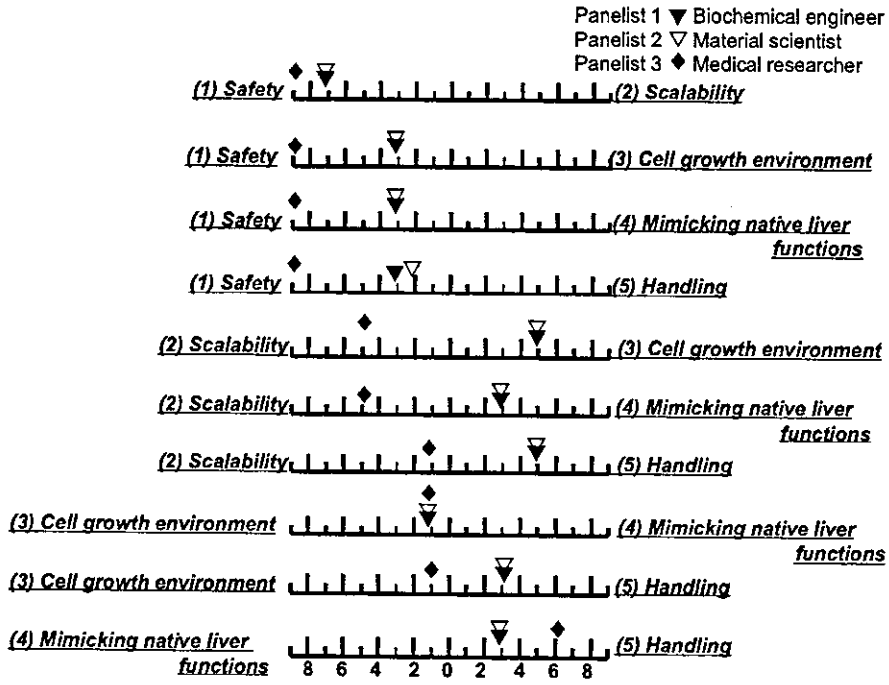

Fig. 3. The results of pairwise comparison in level 2 (functions required for the bioreactor).

judgments were based on the results of referenced papers [11–27]. We set up the five criteria in third level. However, limited information was available in some criteria (i.e. the information related safety, scalability and handling were limited) because of the limitation of original results in the references. In this third level comparison, we performed the pairwise judgment based on these "limited" information. Therefore, the results of criteria included relative and temporary assessments. Table 3 shows the overall judgment results of these pairwise comparisons. Almost all the CR values were below 0.1 except safety and mimicking liver functions in panelist 3. Therefore, these weight value were not consistent. For the criterion of "safety," the capillary network hollow fiber, which has actually been used for human patients, showed the highest rating value. For "scalability" and "cell growth environment," the radial flow bioreactor and "Cygnus," which have showed good performance in industrial mammalian cell culture processes, had good scores in panelists 1 and 2. On the other hands, panelist 3 evaluated that the MC-PUF/spheroid had a good performance of scalability. "Mimicking native liver functions" is a most important consideration for the replacement of a real liver. The MC-PUF/spheroid module, which showed superior performance for spheroid formation and maintenance, was the most suitable reactor for mimicking liver functions in panelists 1 and 2. For evaluation of handling, panelists 1 and 2 thought that the radial flow reactor and Cygnus were good performance for handling though the panelist 3 evaluated that the only Cygnus was convenient.

Table 2
Rankings for level 2 criteria

Criterion	Weight		
	Panelist 1	Panelist 2	Panelist 3
Safety	0.439	0.404	0.662
Scalability	0.043	0.044	0.139
Cell growth environment	0.135	0.139	0.054
Mimicking liver functions	0.118	0.122	0.038
Handling	0.265	0.291	0.107
CR	0.050	0.032	0.131

The conclusions as to the final overall rankings of the BAL systems in panelists 1 and 2 are shown in Fig. 4. The capillary network hollow fiber is the best selection for a BAL system, but the radial flow and Cygnus bioreactors had comparable scores in panelist 1. In panelist 2, ranked the radial flow bioreactor to the best one but the capillary network hollow fiber and Cygnus had comparable scores. In this comparison, we assume use of the same porcine hepatocytes. The AHP method can be expanded for selection of a suitable BAL system containing different types of cells also determined by using the AHP method. Recently, a variety of suitable materials has been developed for hepatocyte scaffolds to support liver functions [28]. The evaluations of these novel scaffolds should be included in future. In this paper, the ranking of evaluation criteria shown in Table 3 was similar between panelists. However, the reactor evaluation varied with panelists. In order to conclude the various points of view in the pairwise evaluation, it is necessary to organize the "panel expert members" who had various backgrounds

Table 3
Overall results for pairwise comparison in level 3[a]

		(1) Safety	(2) Scalability	(3) Cell growth environment	(4) Mimicking liver functions	(5) Handling
Collagen entrapped hollow fiber	Panelist 1	0.037	0.047	0.041	0.247	0.113
	Panelist 2	0.037	0.047	0.041	0.247	0.113
	Panelist 3	*0.04*	0.031	0.041	*0.249*	0.037
Capillary network hollow fiber	Panelist 1	0.364	0.207	0.086	0.107	0.102
	Panelist 2	0.364	0.207	0.086	0.115	0.102
	Panelist 3	*0.609*	0.139	0.041	*0.289*	0.042
Radial flow reactor	Panelist 1	0.075	0.391	0.409	0.14	0.326
	Panelist 2	0.075	0.391	0.409	0.143	0.326
	Panelist 3	*0.072*	0.158	0.206	*0.206*	0.177
MC-PUF/spheroid	Panelist 1	0.122	0.08	0.132	0.303	0.074
	Panelist 2	0.122	0.08	0.132	0.281	0.074
	Panelist 3	*0.068*	0.492	0.289	*0.145*	0.089
Packed-bed with PVF	Panelist 1	0.201	0.115	0.12	0.091	0.149
	Panelist 2	0.201	0.115	0.12	0.098	0.149
	Panelist 3	*0.048*	0.04	0.134	*0.041*	0.177
Cygnus	Panelist 1	0.201	0.16	0.212	0.112	0.237
	Panelist 2	0.201	0.16	0.212	0.115	0.237
	Panelist 3	*0.162*	0.139	0.289	*0.07*	0.478
CR	Panelist 1	0.073	0.079	0.054	0.083	0.078
	Panelist 2	0.073	0.079	0.054	0.075	0.078
	Panelist 3	*0.124*	0.066	0.074	*0.16*	0.067

[a] The results in CR > 0.1 are in italics.

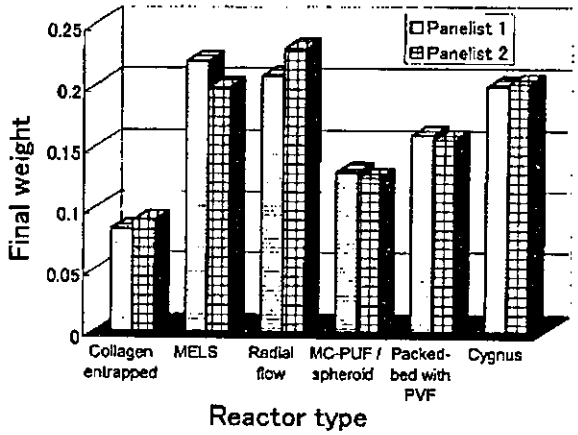

Fig. 4. Final overall rankings of BAL systems using AHP method (panelists 1 and 2).

(i.e. medical doctor, physician, surgeon, biologist, chemical engineer and so on). Using AHP methodology, it is possible to conclude such various different evaluations into hierarchical constructed criteria. The AHP method should be an appropriate tool for evaluating future BAL systems.

4. Conclusion

To develop a method of evaluation in tissue engineering and regenerative medicine, we applied the AHP method to evaluate tissue engineering reactors and different media. In the case of reactor selection for a BAL system, we selected five criteria and successfully ranked six BAL bioreactors using the AHP method.

Acknowledgements

We thank Dr. S. Enosawa for evaluation of the BAL system using AHP analysis.

References

[1] T.L. Saaty, The Analytic Hierarchy Process, McGraw-Hill, New York, 1980.
[2] G. Stephanopoulos, C. Han, Intelligent systems in process engineering, Comput. Chem. Eng. 20 (1996) 743–791.
[3] P.J. Hanratty, B. Joseph, Decision-making in chemical engineering and expert systems: application of the analytic hierarchy process to reactor selection, Comput. Chem. Eng. 16 (1992) 849–860.
[4] D.R. Cook, S. Staschak, W.T. Green, Equitable allocation of livers for orthotropic transplantation: an application of the analytic hierarchy process, Eur. J. Oper. Res. 48 (1990) 49–56.
[5] J.M. Hummel, W. van-Rossum, G.J. Verkerke, G. Rakhorst, Medical technology assessment: the use of the analytic hierarchy process as a tool for multidisciplinary evaluation of medical devices, Int. J. Artif. Organs 23 (2000) 782–787.
[6] A.J. Strain, J.M. Neuberger, A bioartificial liver—state of the art, Science 295 (2002) 1005–1009.
[7] I. Jasmund, A. Bader, Bioreactor developments for tissue engineering applications by the example of the bioartificial liver, Adv. Biochem. Eng. Biotechnol. 74 (2002) 99–109.

[8] A.G. Sheil, Xenogeneic bioartificial liver support: where are we now, Transplant. Proc. 34 (2002) 2493–2495.
[9] H.O. Jauregui, The technology of biological extracorporeal liver assist devices: from infancy to adolescence, Artif. Organs 21 (1997) 1163–1168.
[10] H. Bismuth, J. Figueiro, D. Samuel, What should we expect from a bioartificial liver in fulminant hepatic failure? Artif. Organs 22 (1998) 26–31.
[11] D. Mobest, R. Mertelsmann, R. Henschler, Serum-free ex vivo expansion of CD34(+) hematopoietic progenitor cells, Biotechnol. Bioeng. 60 (1998) 341–347.
[12] F.J. Wu, J.R. Friend, A. Lazar, H.J. Mann, R.P. Remmel, F.B. Cerra, W.S. Hu, Hollow fiber bioartificial liver utilizing collagen entrapped porcine hepatocyte spheroids, Biotechnol. Bioeng. 52 (1996) 34–44.
[13] W.S. Hu, J.R. Friend, F.J. Wu, T. Sielaff, M.V. Peshwa, A. Lazar, S.L. Nyberg, L.K. Hansen, R.P. Remmel, F.B. Cerra, Development of a bioartificial liver employing xenogeneic hepatocytes, Cytotechnology 23 (1997) 29–38.
[14] I.M. Sauer, J.C. Gerlach, Modular extracorporeal liver support, Artif. Organs 26 (2002) 703–706.
[15] L.M. Flendrig, A.A. te Velde, R.A.F.M. Chamuleau, Semipermeable hollow fiber membranes in hepatocyte bioreactors: a prerequisite for a successful bioartificial liver? Artif. Organs 21 (1997) 1177–1181.
[16] I.M. Sauer, N. Obermeyer, D. Kardassis, T. Theruvath, J.C. Gerlach, Development of a hybrid liver support system, Ann. NY Acad. Sci. 944 (2001) 308–319.
[17] J.P. Tharakan, P.C. Chau, A radial flow hollow fiber bioreactor for the large-scale of mammalian cells, Biotechnol. Bioeng. 28 (1986) 329–342.
[18] H. Yoshida, S. Mizutani, H. Ikenaga, Scale-up of interleukin-6 production by BHK cells using a radial-flow reactor packed with porous glass beads, J. Ferment. Bioeng. 84 (1987) 279–281.
[19] S. Mizutani, Bioreactor with radial flow-replenishing system for fermentation, Japanese Patent 09000240 (1997).
[20] T. Matsuura, M. Kawada, S. Hasumura, S. Nagamori, T. Obata, M. Yamaguchi, Y. Hataba, H. Tanaka, H. Shimizu, Y. Unemura, K. Nonaka, T. Iwaki, S. Kojima, H. Aizaki, S. Mizutani, H. Ikenaga, High density culture of immortalized liver endothelial cells in the radial-flow bioreactor in the development of an artificial liver, Int. J. Artif. Organs 21 (1998) 229–234.
[21] H. Mizumoto, M. Hayakami, K. Nakazawa, H. Ijima, K. Funatsu, Formation of cylindrical multicellular aggregate (cylindroid) and expression of liver specific functions of primary rat hepatocytes, Cytotechnology 31 (1999) 69–75.
[22] K. Funatsu, H. Ijima, K. Nakazawa, Y. Yamashita, M. Shimada M, K. Sugimachi, Hybrid artificial liver using hepatocyte organoid culture, Artif. Organs 25 (2001) 194–200.
[23] N. Ohshima, K. Yanagi, H. Miyoshi, Packed-bed type reactor to attain high density culture of hepatocytes for use as a bioartificial liver, Artif. Organs 21 (1997) 1169–1176.
[24] H. Miyoshi, K. Yanagi, H. Fukuda, N. Ohshima, Long-term continuous-culture of hepatocytes in a packed-bed reactor utilizing porous resin, Biotechnol. Bioeng. 43 (1994) 635–644.
[25] T.H. Yang, H. Miyoshi, N. Ohshima, Novel cell immobilization method utilizing centrifugal force to achieve high-density hepatocyte culture in porous scaffold, J. Biomed. Mater. Res. 55 (2001) 379–386.
[26] S. Enosawa, T. Miyashita, H. Tanaka, X.K. Li, S. Suzuki, H. Amemiya, T. Omasa, K. Suga, T. Matsumura, Prolongation of survival of pigs with ischemic liver failure by treatment with a bioartificial liver using glutamine synthetase transfected recombinant HepG2, Transplant. Proc. 33 (2001) 1945–1947.
[27] S. Enosawa, T. Miyashita, S. Suzuki, X.K. Li, M. Tsunoda, H. Amemiya, M. Yamanaka, S. Hiramatsu, N. Tanimura, T. Omasa, K. Suga, T. Matsumura, Long-term culture of glutamine synthetase-transfected HepG2 cells in circulatory flow bioreactor for development of a bioartificial liver, Cell Transplant 9 (2000) 711–715.
[28] T. Miyashita, S. Enosawa, S. Suzuki, A. Tamura, H. Tanaka, H. Amemiya, T. Matsumura, T. Omasa, K. Suga, T. Aoki, Y. Koyanagi, Development of a bioartificial liver with glutamine synthetase-transduced recombinant human hepatoblastoma cell line, HepG2, Transplant. Proc. 32 (2000) 2355–2358.

POLYMERS FOR ADVANCED TECHNOLOGIES
Polym. Adv. Technol. 2004; 15: 232–243
Published online in Wiley InterScience (www.interscience.wiley.com). DOI: 10.1002/pat.473

PAT

Real time monitoring of drug metabolic enzyme response inside human hepatoma GS-3A4-HepG2 cells by means of electrochemical impedance measurement

Masaaki Kobayashi[1], Nobuhiro Sugihara[1], Hirohiko Ise[1], Takeshi Omasa[2] and Naoki Negishi[1]*

[1]Graduate School of Medicine, Shinshu University, 3-1-1 Asahi, Matsumoto, Nagano 390-8621, Japan
[2]Graduate School of Engineering, Osaka University, 2-1 Yamada-Oka, Suita, Osaka 565-0871, Japan

Received 3 September 2003; Revised 8 October 2003; Accepted 14 October 2003

Cytochrome P-450s (CYPs) are important biopolymers for the maintenance of cellular function. If metabolic activity of the CYP in the cells can be estimated, so can the function of metabolism, which is closer to the organism. In this research, the method of measuring the drug metabolic activity inside the cell by making use of an electrochemical technique was examined. Human hepatoma GS-3A4-HepG2 cells of which the cytochrome P-4503A4 (CYP3A4) drug metabolic activity is found to be the same as that of primary hepatocytes were used in the experiment. The GS-3A4-HepG2 cells were cultured on an indium-tin oxide (ITO) electrode until they became confluent. Substrate testosterone and inhibitor ketoconazole of CYP3A4 were exposed to cells cultured on an ITO electrode, and the reaction was observed by noting the electrochemical impedance measurement. Impedance was decomposed into the resistance component and the reactance component, and each was examined in detail. As a result, according to testosterone concentration change, there was a remarkable time change in the reactance component. A similar impedance measurement was done by using human hepatoma HepG2 cells in which the drug metabolic activity had extremely decreased. Nevertheless, no time change in the reactance component that was noticed in GS-3A4-HepG2 cells was observed. Next, the amount of metabolite in the solution after impedance measurement was measured by means of liquid chromatography-tandem mass spectroscopy (LC-MS/MS). In the experiment with GS-3A4-HepG2 cells, a testosterone concentration-dependent correlation was observed between the reactance component change and the amount of metabolite. But, in the impedance measurement by ketoconazole, the change in reactance components was not observed in either the GS-3A4-HepG2 cells or the HepG2 cells. Ketoconazole and the heme iron in CYP3A4 effect the coordination bond, but ketoconazole was not metabolized by CYP3A4. It was confirmed that the time change in the reactance component which was caused by the testosterone was detected neither in the cells that take up the substrate, nor in the coordination bond between the CYP enzyme and the drug. Therefore, the time change in the remarkable reactance component observed by this electrochemical impedance measurement is dependent on drug metabolic activity. An electrochemical drug metabolic activity measuring method with the human hepatoma GS-3A4-HepG2 cells was able to be established. Copyright © 2004 John Wiley & Sons, Ltd.

KEYWORDS: bioengineering; biomaterials; electrochemistry; sensors; cytochrome P-4503A4(CYP3A4)

INTRODUCTION

Cytochrome P-450s (CYPs) are hemoprotein enzymes and are important biopolymers for the maintenance of cellular function. CYPs play a significant role in important biochemical processes, such as vitamin D_3 activation[1–3] and steroid hormone biosynthesis and degradation.[4,5] They are also important for the oxidative metabolism of xenobiotics[6,7] and for drug metabolism.[8,9] CYPs play an active part when the heme iron inside the enzyme receives the electron, and the CYP redox cycle catalyzes the mono-oxygenation reaction of the drug. CYPs are therefore heme-containing mono-oxygenases.[10]

It is important for pharmacological and toxicological evaluation to measure the energy of binding of drugs to CYPs and/or the metabolic activity of CYPs. Various methods have been tried and assessed in order to detect these reactions. When CYPs show drug metabolic activity,

**Correspondence to*: N. Negishi, Graduate School of Medicine, Shinshu University, 3-1-1 Asahi, Matsumoto, Nagano 390-8621, Japan.
E-mail: negishi@sch.md.shinshu-u.ac.jp

the excitation wavelength of the heme iron in the enzyme shifts from 412 to 390 nm due to bonding of the drug to the heme iron. In addition, the energy level of the heme iron changes from 340 to 170 meV after connection of the substrate to the heme iron.[11–13] These reactions can be measured optically. Moreover, there are other methods to measure metabolic activity indirectly by determining the amount of metabolite. For instance, metabolite quantity has been measured by means of high performance liquid chromatography (HPLC) analysis,[14,15] and inhibitory effects of various compounds on CYPs have been assessed by using fluorometric substrates.[16] However, these methods entail complicated processes and it takes a long time to obtain the results. In addition, the method to monitor the energy level of the heme iron cannot determine whether the metabolite was generated or not, while the method to measure the amount of metabolite cannot directly evaluate the metabolic activity of CYP.

In a number of studies, the drug activity of an enzyme placed on an indium-tin-oxide (ITO) electrode was measured electrochemically to test receipt of the electron of the enzyme, because metabolic activity increases when the heme iron in the CYP receives the electron.[17–19] The CYP redox reaction was then measured by means of cyclic voltammetry (CV) and the changes in measurement were related to enzymatic activity of CYP.[19] CV measurement can analyze this enzymatic activity as a single unit, but it is difficult to obtain information related to enzymes which are relatively close to the vital reaction. Thus, metabolic activity measurement by means of cells has been researched, because cells possess the sequential function of metabolism which is closer to the organism than to the single enzyme unit.[20–22] The cell is a complex which contains all the conditions required for drug metabolic reaction of CYPs. If metabolic activity of the CYP in the cell can be estimated, so can the function of metabolism, which is closer to the organism. However, there have been no reports to indicate that the changes in enzyme activity inside the cell can be measured.

In the study reported here, electrochemical techniques, which have many advantages, such as simple and easy procedures and a low error margin as a result of multiplication, were used to develop a method for detecting the CYP redox reaction inside the cell. GS-3A4-HepG2 cells from a human hepatoma,[23] which have the same cytochrome P-4503A4 (CYP3A4) activity as the primary hepatocyte, were used for the measurement. The reaction between testosterone, which is the substrate of CYP3A4, and GS-3A4-HepG2 cells was investigated by comparing the electric parameters. The substrate testosterone is used as the most general reagent to evaluate the activity of CYP3A4. Therefore GS-3A4-HepG2 cells were exposed to the testosterone cultured in the confluent monolayer on an ITO electrode, and the physicochemical changes inside the cells were identified with the electrochemical impedance method. If the information obtained with this method does not only effect monitoring of the morphological changes in the cells, but can also monitor the metabolic reaction of CYP3A4 in the cells and the drug in real time, it can be expected to be effective for the development of new medicines. By applying the impedance measuring method used in electrochemistry, it was possible to show that the detection of physico-chemical changes inside the cells is achievable.

EXPERIMENTAL

Chemicals and reagents

The RDF (HO) culture medium extracts glutamine and glucose from the mixed culture medium of RPMI1640: DMEM:F12 = 2:1:1 which was purchased from Wako Pure Chemical Industries, Ltd. Dulbecco's modified Eagle's medium (DMEM) was purchased from SIGMA. PSN Antibiotic Mixture (PSN) was purchased from GIBCO. The Leibovitz's L-15 Medium (L-15) of the CO_2 non-dependent culture medium was purchased from GIBCO. Sterile Foetal Bovine Serum (FBS) was purchased from MoreGate. Testosterone was purchased from Wako Pure Chem. Ketoconazole was purchased from Daiichi Pure Chemicals Co., Ltd. Dimethylsulfoxide (DMSO) was purchased from Daiichi Pure Chemicals Co., Ltd. Penicillin G Sodium Salt and Streptomycin Sulfate were purchased from Wako Pure Chemical Industries. Zeocin was purchased from Invitrogen. Glucose and $NaHCO_3$ were purchased from Daiichi Pure Chemicals Co., Ltd. Glutamine was purchased from GIBCO.

Electrode preparation and measuring apparatus

The core components of the experimental apparatus are the impedance measurement container shown in Fig. 1(A). The principal components of the impedance measurement container are the ITO electrode and the cloning ring made of glass in the form of a cylinder. The ITO sheet glass (30 cm × 30 cm) was purchased from the Nippon Sheet Glass Co., Ltd and it was cut into 1.5 cm × 1.5 cm size pieces and used as ITO electrodes. The cylindrical cloning ring with an external diameter of 1.2 cm, an inside diameter of 1 cm and a height of 1 cm (purchased from IWAKI) was arranged at the center of the electrode side where ITO was evaporated. The cloning ring and ITO electrode were fixed with epoxy adhesives. Consequently, the impedance measurement container had a base area of 0.785 cm^2 and a volume of 0.785 cm^3. Conductivity and visibility are securable enough by using an ITO electrode for cells adhesion portion. Verifying that the ITO electrode and the cloning ring had adhered completely, the impedance measurement container was sufficiently washed by ultrasonic cleaning and sterilized by the usual autoclave technique.

The electrode composition used the three-electrode method most generally used for electrochemistry measurement.[17–19] An ITO electrode at the bottom of an impedance measurement container was used as a working electrode, and it was connected to the measurement machine by means of a platinum wire 1 mm in diameter. The cells were cultured on this ITO electrode. For the reference electrode and counter electrode 1 mm diameter platinum wires were used, respectively. In order to increase the surface area and to keep the distances from the reference electrode equal, the counter electrode was processed circular with a 6.4 mm inner diameter, as shown in Fig. 1(A), and was arranged with the reference electrode at the center. Moreover, each electrode was fixed in position with a cork made from silicone for good insulation so that the distances between the ITO electrode and reference electrode and counter electrode could be kept

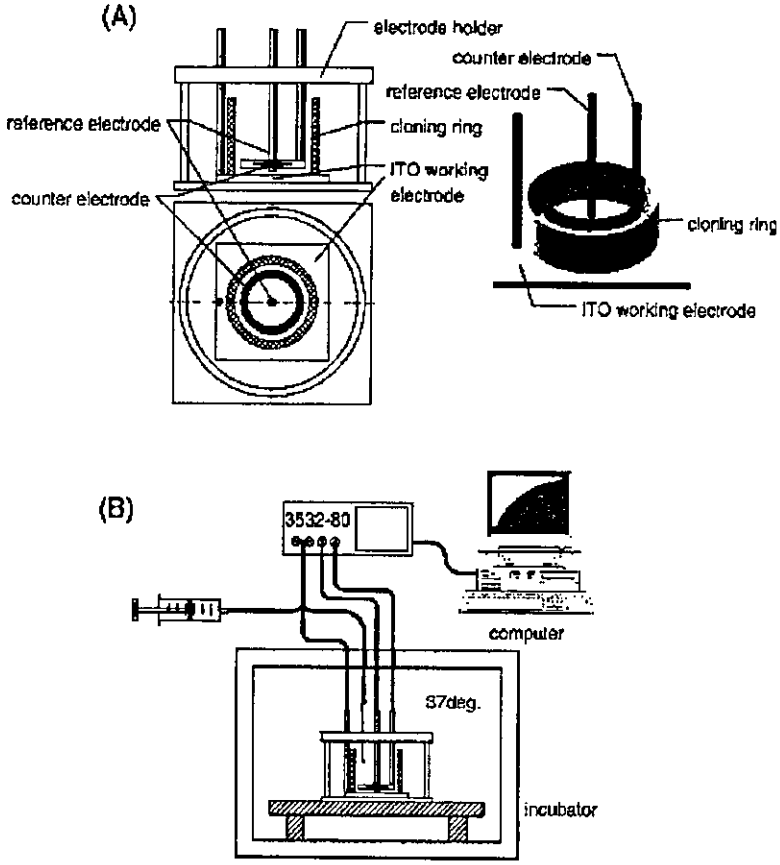

Figure 1. (A) Schematic drawing of the impedance measurement container. Details of container construction are given in Experimental section. (B) Experimental apparatus for recording impedance data. A measuring container as shown in (A) is fixed on a small metal table with a built-in plastic electrode holder that serves to contact the platinum electrodes. The electrodes are connected to the impedance meter (3532-80). To apply the substances under study, a sterile syringe is used to add the medium above the cell layer with minimal mechanical or thermal disturbance.

at 0.5 mm and 1.0 mm, respectively. During an experiment the impedance measurement container was placed in a 37°C incubator in atmosphere. The incubator was placed near the impedance meter to minimize parasitic effects of the connecting cables (Fig. 1B). The impedance measurement container was fixed in position on the metal stand. Each electrode was connected to the equipment with a suitable metallic clip. The syringe shown in Fig. 1(B) was used to administer the compounds suited to the cells under investigation.

Cell culture

GS-3A4-HepG2 culture method

A human hepatoma GS-3A4-HepG2 cell line with CYP3A4 activity of same strength as the primary hepatocyte was established by Omasa *et al.*[23] GS-3A4-HepG2 cells were suspended in the FBS solution to which was added 10% (v/v) DMSO. The cells were cryopreserved at −150°C until use. Just before use, the cryopreserved cells were thawed in a thermostat water bath at a temperature of 37°C. The cells were seeded 3×10^5 cells/well in the impedance measurement container (base area of 0.785 cm^2), and were grown to confluence in a humidified incubator with 5% CO_2 at 37°C. The RDF (HO) medium served as the culture medium and was supplemented with 10% (v/v) FBS, 2.576 g/l glucose, 2 g/l $NaHCO_3$, 0.333 g/l glutamine, 58.8 mg/l penicillin G, 120 ml/l streptomycin, and 0.2% (v/v) Zeocin and was used 500 µl/well. The culture medium was changed every 12 hr, and the morphology of the cells was observed by means of a microscope. The impedance measurement container in which the cells on the ITO electrode proliferated to confluence was used for the impedance measurement. In order to keep the condition of the cells constant, the culture medium was changed to 500 µl of supplemented RDF (HO) culture medium as described earlier, but without FBS, 12 hr before measurement started.

The HepG2 culture method

The human hepatoma HepG2 cells were purchased from GENTEST, and were preserved and cultivated like the GS-3A4-HepG2 cells, but the DMEM served as the culture and

was supplemented with 1% (v/v) PSN and 10% (v/v) FBS. Moreover, 12 hr before the start of measurement, the culture medium was changed to the earlier mentioned supplemented DMEM without FBS.

Impedance measurement and data analysis

The whole system image is shown in Fig. 1(B). A HIOKI 3532-80 Chemical Impedance Meter (HIOKI E.E. Corporation, Japan) was used for the electrochemical impedance measurement. The apparatus was controlled by a computer to RS-232C communication and the frequency was changed from 100 Hz to 1 MHz, and the impedance modulus Z and the phase-shift θ between the voltage and current were measured.

The output terminal voltage of the apparatus was set at 40 mV as the excitation signal ensuring an adequate signal-to-noise ratio and minimal disturbance of the system. On each measurement frequency, two measured values were averaged. Measuring speed was set to slow and increased measuring accuracy. When such a data set was measured, sweeping the frequency from 100 Hz to 1 MHz, took about 1 min. The measurement interval for each frequency was adjusted to 2 min. Impedance Z is a vector. The impedance Z for each frequency was decomposed into the resistance component (R) and the reactance component (X) by using the phase-shift θ, and each component was evaluated. Each component, Z, R and X was evaluated as a percentage of ratio of the standard value based on each measurement just after addition of the drug (time: $t=0$) and each measurement at elapsed time (t). Thereby, external error factors, such as contact resistance at the electrode connection and/or the amount of error due to addition of the solution etc., could cancel out, and minute cell changes could be measured with sufficient sensitivity. A new impedance measurement container was used for each measurement. The reference electrode and the counter electrode were washed by ultrasonic cleaning for 15 min before starting measurements, and error due to impurities adhering to the electrodes was kept to a minimum. All data were measured five times or more for every drug concentration and every batch of cells, respectively, and the average was recorded.

CYP3A4 substrate testosterone reaction experiment

Both GS-3A4-HepG2 cells and HepG2 cells were subjected to electrochemical impedance measurements. Substrate testosterone was dissolved to a 100 mM concentration in DMSO in advance and was kept at −20°C until used. The stock solution was thinned to L-15 culture medium immediately before the experiment. The impedance measurement container in which cells on the ITO electrode proliferated to confluence verified by microscopy was used for the impedance measurement.

The culture medium was changed to FBS additive-free L-15 medium 200 µl, 2 hr before measurement. The impedance measurement container was moved to the inside of the incubator, and a reference electrode and counter electrode were positioned. Each electrode was connected to the impedance meter, and measurement was done without drug addition for 2 hr until the measured value was stabilized in a humidified incubator in atmospheric CO_2 at 37°C. After verifying that the measuring system had stabilized sufficiently, testosterone was dissolved in the L-15 medium so that the final density might become 300, 150, 75, 50 and 0 µM (only DMSO 0.3% v/v), respectively. To apply the substrate under study, a sterile syringe is used to add 200 µl of the medium above the cell layer and the testosterone was exposed to the cells. The reaction between the substrate and cells was measured for 2 hr, and the amount of the last solution used was 400 µl. In each experiment, the final DMSO concentration in the medium was fixed at 0.3% (v/v).

CYP3A4 inhibitor ketoconazole obstruction experiment

Both GS-3A4-HepG2 cells and HepG2 cells were subjected to electrochemical impedance measurements. The inhibitor ketoconazole was dissolved to a 100 mM concentration in DMSO in advance and was kept at −20°C until used. The stock solution was thinned to L-15 culture medium immediately before the experiment. The impedance measurement container in which cells on the ITO electrode proliferated to confluence verified by microscopy was used for the impedance measurement.

The culture medium was changed to FBS additive-free L-15 medium 200 µl, 2 hr before measurement. The impedance measurement container was moved to the inside of the incubator, and the reference electrode and counter electrode were positioned. Each electrode was connected to the impedance meter, and measurement was done without drug addition for 2 hr until the measured value was stabilized in a humidified incubator in atmospheric CO_2 at 37°C. After verifying that the measurement system had stabilized sufficiently, inhibitor ketoconazole was dissolved in the L-15 medium so that the final densities might become 3, 1.5, 0.75, 0.3 and 0 µM (only DMSO 0.3% v/v), respectively. To apply the inhibitor under study, a sterile syringe is used to add 200 µl of the medium above the cell layer and the ketoconazole was exposed to the cells. The reaction between the inhibitor and cells was measured for 2 hr, having used 400 µl of the last solution. In each experiment, the final DMSO concentration in the medium was fixed at 0.3% (v/v).

Testosterone metabolite verification experiment with LC-MS/MS

After the impedance measurement, 400 µl cold methanol of the same quantity as the measured solution was added and the metabolic reaction was stopped. After sufficient agitation, all the measured solutions were gathered. Impurities were precipitated by centrifugation at 15 500 × g for 10 min. The supernatant fluid was extracted and the amount of 6-β-hydroxy testosterone that is a testosterone metabolite was immediately analyzed by liquid chromatography-tandem mass spectroscopy (LC-MS/MS). For metabolite mass spectroscopy verification an Applied Biosystems-MDS Sciex API 3000 triple quadrupole mass spectrometer equipped with a turbo ion spray source working in the positive ion mode was used. The column for HPLC was a Develosil ODS-HG-3 (inner diameter 2 mm × length 50 mm, particle diameter 3 µM) manufactured by Nomura Chemical Co., Ltd. The running buffer consisted of 0.1% acetic acid in water.

The gradient buffer was 100% methanol. The proportion of gradient buffer increased linearly from 10 to 90% of the eluate in 15 min. Aliquots of 10 µl of each sample were loaded onto the column. The column temperature and flow rate were 40°C and 300 µl/min, respectively. The metabolite and their internal standard were detected by means of multiple reaction monitoring (305.3 → 269.0 for 6-β-hydroxy testosterone) operated in a positive ion mode.

RESULTS

General considerations

When the GS-3A4-HepG2 cells and the HepG2 cells were seeded in the impedance measuring container, the cells adhered in 3 hr. After that the respective cells continued proliferation. Moreover, the GS-3A4-HepG2 cells and the HepG2 cells became confluent in up to 48 and 32 hr, respectively. Although the cells were observed with the microscope, morphological cell death inside the impedance measurement container was not observed. And either cell culture for 160 hr or more was possible on the ITO electrode. Morphological changes before and after the impedance measurement were evaluated, and after impedance measurement, the rate of survival of the cells was confirmed by trypan blue dyeing assay. Figure 2 shows micrographs of GS-3A4-HepG2 cells and HepG2 cells. Figure 2(A) and 2(F) are the micrographs before measurement. The micrographs after impedance measurement with a substrate testosterone concentration of

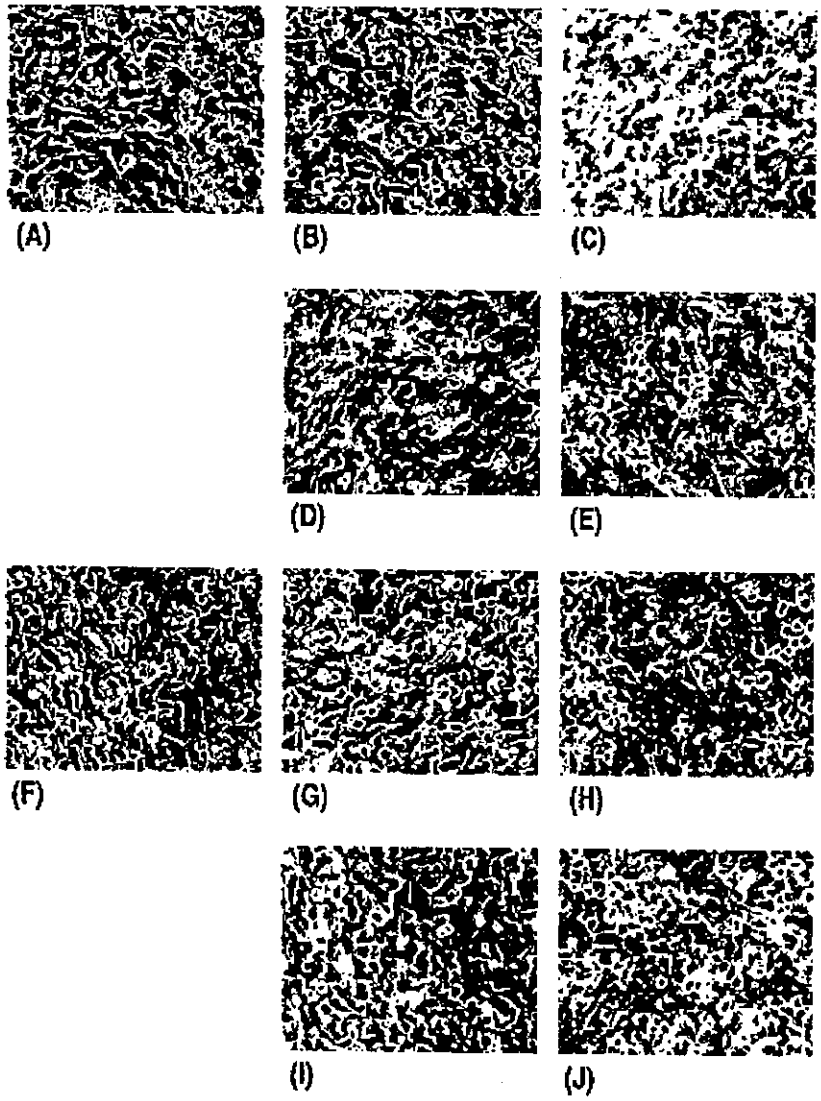

Figure 2. Morphology of GS-3A4-HepG2 cells (A–E) and HepG2 cells (F–J) before and after impedance measurement. And the trypan blue dyeing assay for the cells survivability check after impedance measurement. (A, F) Before impedance measurement; (B, G) after 300 µM testosterone measurement; (C, H) trypan blue dyeing assay after testosterone measurement; (D, I) after 3 µM ketoconazole measurement. (E, J) trypan blue dyeing assay after ketoconazole measurement. The morphological changes in the drugs and in voltage were not ascertained, and the cell death after measurement was not confirmed either. Magnification × 200.

150 μM are shown in Fig. 2(B) and 2(G), and the micrographs obtained with trypan blue dyeing assay after measurement are shown in Fig. 2(C) and 2(H). The micrographs after impedance measurement with an inhibitor ketoconazole concentration of 1.5 μM are shown in Fig. 2(D) and 2(I), and the micrographs obtained with trypan blue dyeing assay after measurement are shown in Fig. 2(E) and 2(J). Figure 2 shows that the cells had few morphological changes after the impedance measurement, and almost all cells which survived were shown by trypan blue dyeing assay. These result show that neither the electric stimulus by impedance measurement nor the drug stimulus caused morphological changes in the cells or affected cell viability.

In electrochemical impedance measurement, the selection of measurement frequency is important. If a measurd frequency which is sensitive to the change inside the cell is found, high sensitivity measurement is possible at that frequency. To find a sensitive frequency, the testosterone was added and the time course change in impedance Z, resistance R and reactance X were measured with an impedance measurement container where the GS-3A4-HepG2 cells are cultured in confluence. As a comparison, similar measurements were done with an impedance measurement container in which the cells were not cultured. In both cases the L-15 medium serves as the bulk electrolyte. Concerning each of the earlier mentioned components, measurement $A(t=0\,\text{hr})$ [where A is either Z, R or X] just after the drug addition was designated as standard at every frequency. $\tau A(t=2\,\text{hr}) = \frac{A(t=2\,\text{hr})}{A(t=0\,\text{hr})}$ was defined as having used the measurement 2 hr after drug addition as $A(t=2\,\text{hr})$ and was compared with the presence of the cells. Impedance Z and resistance R, $\tau Z(t=2\,\text{hr})$ and $\tau R(t=2\,\text{hr})$ hardly change regardless of the existence of cells. At almost every frequency there was a fixed value (data not shown), but at reactance X, $\tau X(t=2\,\text{hr})$ frequency dependence was greatly changed by the cell cultured impedance measurement container. Figure 3 shows the $\tau X(t=2\,\text{hr})$ change according to the existence of cells at each frequency. When substrate testosterone was added when there were no cells, there was no time course or frequency dependence change in $\tau X(t=2\,\text{hr})$. In the condition with GS-3A4-HepG2 cells, $\tau X(t=2\,\text{hr})$ was increased greatly by the frequency band centered on a frequency of 100 kHz. The amount of change was about 7% at the maximum. Consequently, measurement frequency was determined as 100 kHz because the change in $\tau X(t=2\,\text{hr})$ reaches its maximum. From these results, $\tau X(t)$ obtained from reactance X was used for measurement evaluation.

Substrate metabolism reaction experiment

The time course change in $\tau X(t)$ caused by the reaction of GS-3A4-HepG2 cells and substrate testosterone is shown in Fig. 4(A). The horizontal axis shows the time course for 2 hr from just after the addition of testosterone. The vertical axis shows $\tau X(t)$. Figure 4(A) shows that addition of a testosterone concentration of 0 μM (solution only of DMSO (0.3% v/v) which is the solvent for substrate dissolution) is increasing $\tau X(t)$ from just after substrate addition at an almost fixed rate. But when the substrate testosterone was added, another change in $\tau X(t)$ was observed. $\tau X(t)$ increases like the testosterone 0 μM reaction for 10 min after testosterone addition

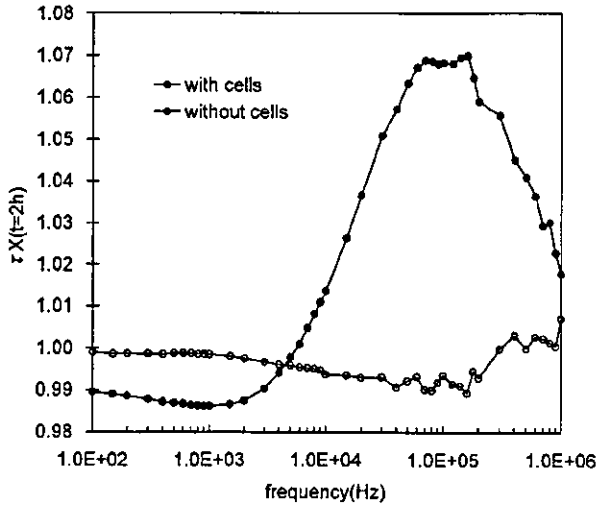

Figure 3. Time dependent typical $\tau X(t=2\,\text{hr})$ spectrum of an ITO electrode covered with a confluent monolayer of GS-3A4-HepG2 cells and of an ITO electrode not covered with cells. When substrate testosterone was added in the condition without cells, there was no time course or frequency dependence change in $\tau X(t=2\,\text{hr})$. Whereas the presence of the cell layer was indicated by the change in $\tau X(t=2\,\text{hr})$ in the frequency band centered on 100 kHz.

regardless of the substrate density. After that, $\tau X(t)$ shows reactions according to the concentration of testosterone for 60 min.

In order to compare the time change in $\tau X(t)$ at each testosterone density, the testosterone concentration 0 μM is designated as the standard. It appeared that the change in $\tau X(t)$ according to the concentration of testosterone reached the maximum at 40 min after adding the substrate. Then, as shown in Fig. 4(A), $\tau X(t)$ at each testosterone concentration 40 min after substrate addition is considered. $\tau X(t)$ at a concentration of 0 μM is set to $\tau 0X$, and $\tau X(t)$ at each concentration is set to $\tau \alpha X$. $\Delta\tau X = |\tau 0X - \tau \alpha X|$ is defined using these.

The change in $\tau X(t)$ at each concentration is confirmed. The tilt angle of $\tau X(t)$ became gradual at a substrate density of 50 μM compared with 0 μM. $\Delta\tau X$ between these concentrations was 0.016. At a substrate concentration of 75 μM, $\tau X(t)$ decreased gradually with time and $\Delta\tau X$ was 0.023. Moreover, with 150 and 300 μM, the reduction in $\tau X(t)$ became more intense and $\Delta\tau X$ was 0.041 and 0.048, respectively. In addition, at 300 μM, $\Delta\tau X$ reached a maximum in 40 min. After that the same $\Delta\tau X$ value was maintained for approximately 20 min. When 60 min or more had passed since substrate testosterone was added, $\tau X(t)$ increased gradually at any substrate concentration. As a result, it was observed that $\Delta\tau X$ was multiplied according to the increase in substrate testosterone density. But, at testosterone concentrations of 150 and 300 μM, the values for $\Delta\tau X$ were 0.041 and 0.048, respectively. Although the testosterone concentration was doubled, $\Delta\tau X$ was not greatly multiplied.

Each measurement solution was extracted and refined after the impedance measurement was terminated, and the amount of 6-β-hydroxy testosterone that was a metabolite of testosterone was confirmed by means of LC-MS/MS. A ratio

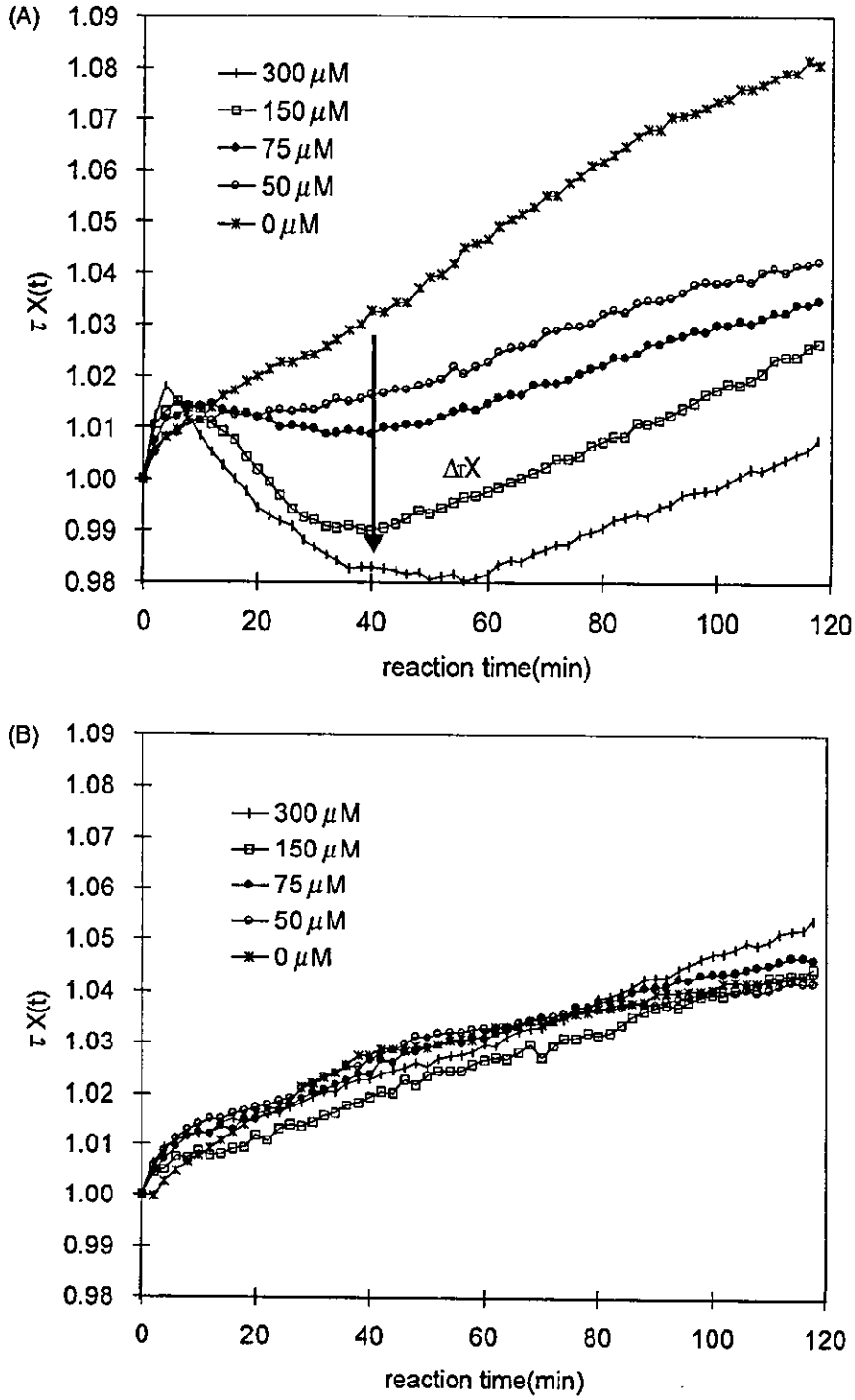

Figure 4. Time course change in $\tau X(t)$ caused by the reaction of (A) GS-3A4-HepG2 cells and (B) HepG2 cells when the cells were treated with 300, 150, 75, 50 and 0 μM (only DMSO 0.3% (v/v)) substrate testosterone. The horizontal axis shows the time course for 2 hr from just after the addition of testosterone. The vertical axis shows $\tau X(t)$. $\Delta\tau X$ is the difference between the $\tau 0X$(40 min) for 0 μM testosterone density and $\tau\alpha X$(40 min) for each testosterone density at 40 min.

of the amount of 6-β-hydroxy testosterone in each concentration that was standardized to the amount of metabolite in 50 μM is shown in Fig. 5. Figure 5 shows that the amount of 6-β-hydroxy testosterone has increased according to the increase in testosterone density. This tendency was observed up to a testosterone concentration of 150 μM, and the substrate density and the amount of metabolite proportionally increased. But, between 150 and 300 μM, the amount of metabolite was not proportionality related, and the tilt angle decreased. $\Delta\tau X$ shown in Fig. 4(A) is plotted in Fig. 5. It

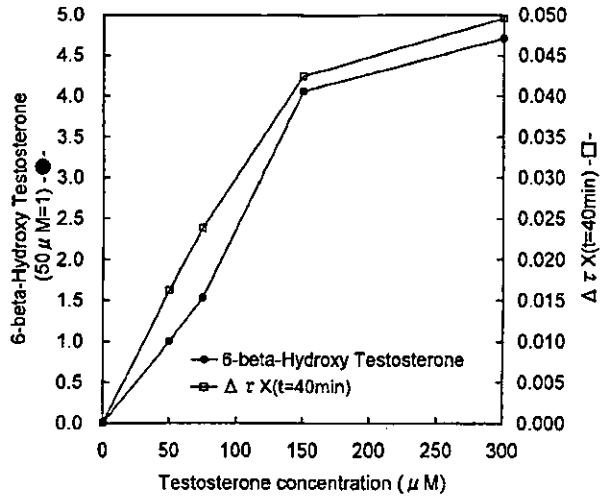

Figure 5. The ratio of the amount of 6-β-hydroxy testosterone in each concentration that was standardized by the amount of metabolism in 50 μM (●). The change in $\Delta\tau X$ (□), is shown in Fig. 4(A). The amount of testosterone metabolite has increased as the testosterone concentration rises and the same tendency was observed in $\Delta\tau X$.

becomes a straight line as shown in Fig. 5. This shows a similar change to the concentration dependent change in the amount of metabolite. Therefore, a correlation between the $\Delta\tau X$ impedance measurement and the amount of metabolite obtained in the LC-MS/MS experiment was confirmed.

A similar testosterone metabolism experiment was done on HepG2 cells that have low drug metabolizing ability. As shown in Fig. 4(B), but there was no change in $\Delta\tau X$ accompanying the increase in the testosterone concentration as shown in Fig. 4(A). $\tau X(t)$ increased almost constantly at every testosterone concentration. Next, each measurement solution was extracted and refined, and the amount of metabolite was measured by LC-MS/MS, but the metabolite was not detected regardless of the testosterone concentration (data not shown).

Ketoconazole inhibition experiment

The redox reaction of the heme iron originates after the coordination bond of the substrates and the heme iron in the enzyme, and the drug metabolic reaction by CYP3A4 progresses. The coordination bond of ketoconazole and the heme iron in the enzyme is reversible, and the reaction after the coordination bond hardly progresses.[24] Then, the cells were exposed to the inhibitor ketoconazole, and the change in $\tau X(t)$ was evaluated. If the same change as in the testosterone experiment was observed, there would be a change in $\tau X(t)$ when monitoring the cells take up of a drug or/and the coordination bond of the enzyme and the drug. However, the same change was not observed, the change in $\tau X(t)$ was monitored for the drug metabolic reaction included the redox reaction of the heme iron.

A time course change in $\tau X(t)$ caused by the reaction of GS-3A4-HepG2 cells and inhibitor ketoconazole is shown in Fig. 6(A). The horizontal axis shows the time course for 2 hr from just after adding ketoconazole. The vertical axis shows $\tau X(t)$. The time course change in $\tau X(t)$ when the ketoconazole concentration is changed from 3 to 1.5, 0.75, 0.3 and 0 μM is shown in Fig. 6(A). The $\tau X(t)$ value increased at a constant rate regardless of the ketoconazole concentration. No remarkable concentration dependence change in $\tau X(t)$ was detected. Moreover, a similar inhibitor ketoconazole experiment was conducted to examine the HepG2 cells. Figure 6(B) shows the result. In this case no ketoconazole dependence change in $\tau X(t)$ was detected at all.

DISCUSSION

When the GS-3A4-HepG2 cells were exposed to testosterone, the time course change in $\tau X(t)$ was found to be concentration dependent, and the correlation was confirmed to depend on the increase in $\Delta\tau X$ and substrate concentration (Fig. 4A). The cause of being assumed that the change in $\tau X(t)$ detects the alteration of the measurement solution composition by metabolism. Nevertheless, $\tau X(t)$ increased for about the first 10 min regardless of the substrate concentration as shown in Fig. 4(A). Afterwards $\tau X(t)$ decreased until 60 min dependent on the substrate concentration. Thereafter $\tau X(t)$ increased continuously at any density. The substrate density decreases due to metabolism with the passage of time, and, conversely, the amount of the metabolite increases with the passage of time. The solution composition change in the medium was only a unidirectional change with the passage of time. Consequently a complex change in $\tau X(t)$ in a short time and a simple change in the measurement solution composition were unrelated. No remarkable change in the cells was detected in microscopic observation and trypan blue dyeing assay. Therefore, no morphological change or death of cells caused by drug stimulus was found. And there was no cell multiplication. And, as shown in Fig. 4(B), In the experiment on HepG2 cells, no change in $\tau X(t)$ according to a change in the substrate concentration was observed, nor in the experiment in which the cells were exposed to the inhibitor ketoconazole (shown in Fig. 6), was a change in $\tau X(t)$ with the change in the inhibitor concentration observed. And also no change in the cells were observed under the microscope after drug stimulation (for instance intracellular or intercellular volume change, changes in cell adhesion, etc.).

As shown in Fig. 5, up to a testosterone concentration of 150 μM, $\Delta\tau X$ and testosterone density are proportionally related. But at a testosterone concentration of 150 μM or more, the increase in substrate density and $\Delta\tau X$ are not proportionally related, but the inclination of $\Delta\tau X$ becomes weaker. The amount of metabolite obtained in the LC-MS/MS experiment was confirmed. Even in the metabolite measurement experiment with the LC-MS/MS, up to a testosterone concentration of 150 μM, the amount of metabolite and the testosterone concentration have a proportional relationship, but above a testosterone concentration of 150 μM, the amount of substrate metabolite was saturated and the inclination of the metabolite becomes weaker. Because these two results correspond, it is seen that there is an interrelationship between $\Delta\tau X$ and LC-MS/MS in the metabolic quantity.

For comparison, the same testosterone metabolite experiment was done to observe the change in $\Delta\tau X$ by using HepG2 cells in which the drug metabolic activity was extremely

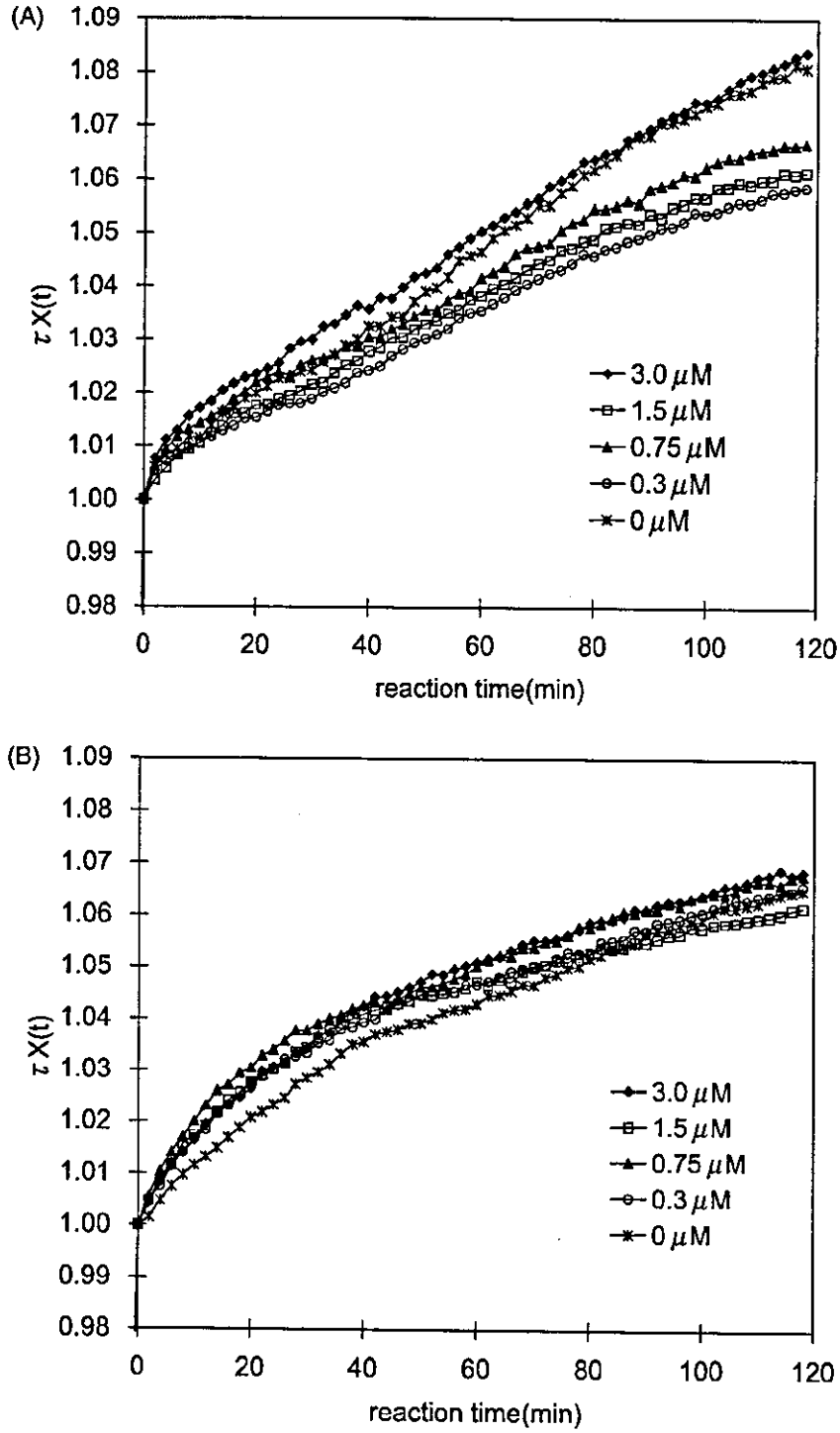

Figure 6. The time course change in $\tau X(t)$ caused by the reaction of (A) GS-3A4-HepG2 cells and (B) HepG2 cells when the cells were treated with 3, 1.5, 0.75, 0.5 and 0 μM (only DMSO 0.3% (v/v)) inhibitor ketoconazole. The horizontal axis shows the time course for 2 hr from just after the addition of ketoconazole. The vertical axis shows $\tau X(t)$. Each cell change in $\tau X(t)$ only increased regardless of the inhibitor ketoconazole density.

decreased. As Fig. 4(B) shows, no change in $\tau X(t)$ depending on the substrate concentration with the passage of time was confirmed, and $\tau X(t)$ only increased at a fixed rate. Although the amount of metabolite was measured by LC-MS/MS, no metabolite was detected regardless of the substrate concentration (data not shown). This result leads to a correlation between the change in $\Delta\tau X$ in impedance measurement and the metabolite content measured by LC-MS/MS.

The main differences in the drug metabolism processes of the GS-3A4-HepG2 cells and the HepG2 cells are the

existence of the activity of CYP3A4. It was regarded that the time course change in $\tau X(t)$ depending on the substrate testosterone density is based on the drug metabolic reaction between the CYP3A4 enzyme and the substrate testosterone. Therefore, the results of these experiments suggest that the metabolic activity of the cells depending on drug density can be detected by the change in $\Delta\tau X$ according to the substrate testosterone concentration. Specifically, the increase in $\Delta\tau X$ is reflected in the increase in metabolic activity, and the decrease in the $\Delta\tau X$ indicates a reduction in the metabolic activity. Therefore, as shown in Fig. 5, it is expected that the metabolic activity of the GS-3A4-HepG2 cells depends on the drug density to the limit of metabolic capacity. As up to a testosterone concentration of 150 μM, the cells respond to the increase in drug density by increasing the metabolic activity, which was detected by the change in $\Delta\tau X$. And substrate metabolism around the cells is completed at the almost same time regardless of substrate density. The change in $\tau X(t)$ increases after about 40 min regardless of the substrate density. This explains how all the substrate testosterone around cells was metabolized in about 40 min and the metabolic response was completed. So the metabolic activity of the cells decreases. After all the substrate testosterone around cells was metabolized and the metabolic response was completed, $\tau X(t)$ started to increase. This can explain why $\tau X(t)$ increases at every concentration after 40 min. Moreover, at a substrate testosterone density of 300 μM, cell metabolic capability reaches its limit. Therefore, the metabolism of the substrate around the cells was not terminated in 40 min and the metabolism continues for a while. The change in $\Delta\tau X$ also reached its maximum in 40 min. The maximum level was maintained for 20 min after that, and this portion may have detected metabolic continuation.

The inhibitor ketoconazole bonds to the heme iron in the CYP3A4 enzyme and inhibits enzyme revitalization. The coordination bond between ketoconazole and the heme iron in the enzyme is reversible, and the reaction after coordination bonding hardly progresses. If the same change as in the substrate testosterone experiment is observed in the inhibitor ketoconazole experiment, there would be a change in $\tau X(t)$ when monitoring the cells take up of a substrate or/and the coordination bond of the enzyme and the drug. But in the present experiment, $\tau X(t)$ increased at constant rate regardless of the ketoconazole concentration. No remarkable concentration dependent change in $\tau X(t)$ was detected. Although the $\tau X(t)$ of the HepG2 cells was also compared by conducting the same experiment (Fig. 6B), no change in $\tau X(t)$ was detected, namely the $\tau X(t)$ in both the GS-3A4-HepG2 cells and the HepG2 cells was altered to almost the same degree. Therefore, it was verified that $\tau X(t)$ was detected neither in the cells that take up the substrate, nor in the coordination bond between the enzyme and the drug. The results suggested that the change in $\tau X(t)$ was monitored in the drug metabolic reaction including the redox reaction of the heme iron.

Next, the electrochemical implications of the measured values are considered. Figure 7 shows an electrochemical equivalent circuit in confluent cultured of the cell on the electrode in this measurement. Microscopic observation of this model (Figure 7(A)), shows complex equivalent circuits. The electrical properties of the naked electrode in contact

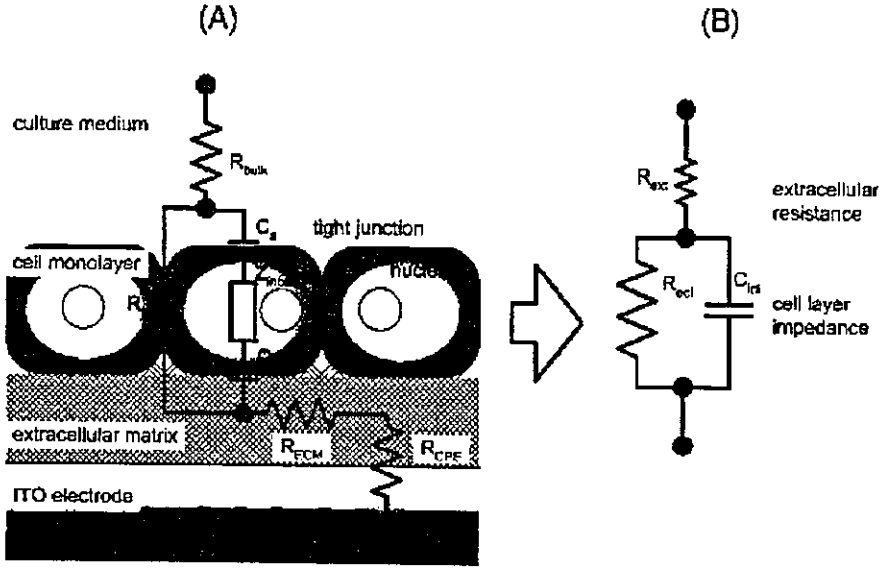

Figure 7. Equivalent circuit representations for the confluent monolayer of GS-3A4-HepG2 cells. (A) Microscopic equivalent circuit (R_{bulk}, resistance of the L-15 medium; C_a, C_b, capacitance of the apical (subscript a) or basal (subscript b) cell membrane; Z_{incell}, impedance of intracellular element; R_{tj}, resistance of the tight junctions; R_{ECM}, resistance of extracellular matrix; R_{CPE}, resistance due to a constant-phase element of the ITO electrode). (B) Macroscopic equivalent circuit (R_{ext}, resistance of the extracellular element; R_{ecl}, resistance of the intercellular element; C_{icl}, capacitance of the cell monolayer).

with the bulk electrolyte are described by a series combination of a constant-phase element (CPE) that accounts for the impedance associated with the electrode/electrolyte interface,[25–27] and a resistance due to the conductivity of the bulk medium (R_{bulk}). The cells which were adhered to the extracellular matrix (R_{ECM}) on the ITO electrode require some additional impedance elements, an intracellular impedance (Z_{incell}), cell membrane capacitors (C_a, C_b), a resistor for the tight junction (R_{tj}) arranged in complex combination, that account for the electrical properties of the cell.[28] In order to detect minute changes in the ITO electrode with sufficient sensitivity, a three-electrode method was used. Therefore, the influence of the counter electrode and reference electrode was negligible in this equivalent circuit. In this article the focusing reaction was the intracellular metabolic response between drugs and metabolism enzymes. Therefore, it is necessary to pay attention to the parameter that penetrates a cell membrane and changes with the influences of intracellular disturbance. In macroscopic observation of the model (Fig. 7B), the electrical properties of constant extracellular resistance and cell layer impedance are shown by a series combination. The constant properties of extracellular resistance include a CPE, a bulk medium (R_{bulk}) and extracellular matrix (R_{ECM}). The properties of the cells layer were a capacitor C and a resistor R arranged in parallel, that account for the resistive and capacitive properties of the cell monolayer as an insulation layer. Evaluation has already been proven in many experiments.[27] From a macroscopic equivalent circuit, the formula for impedance Z near the electrode is as follows:

$$Z = \frac{R_{ecl}}{1 + (\omega R_{ecl} C_{icl})^2} + R_{ext} - j\frac{\omega R_{ecl}^2 C_{icl}}{1 + (\omega R_{ecl} C_{icl})^2} \quad (1)$$

Where j is the imaginary unit and ω is the angler frequency. In many reports, impedance Z is used as an evaluation value. The change in impedance Z, morphological change in adhesion, and expansion, etc. of cells on the electrodes is observable,[25,26] but impedance is a vector ingredient and can be decomposed into a resistance ingredient and a reactance ingredient. By observing reactance, it is expected that the electric charge movement or/and energy change in the ion and enzyme within a cell membrane (i.e. intracellular) will be detected. In this analysis, the reactance ingredient for each time is calculated as a ratio based on the reactance ingredient X(0) just after drug addition. When the reactance after time t progress from drug addition is defined as $X(t)$, the reactance ratio $\tau X(t)$ is expressed with the following formula:

$$\tau X(t) = \frac{X(t)}{X(0)} \quad (2)$$

The component that changes depending on time progress is only capacitance influenced by the intracellular alteration. When capacitances in X(0) and $X(t)$ are assumed to be C_0 and C_t, respectively, the reactance in eq. (1) is substituted in eq. (2). The function is given as:

$$\tau X(t) = \frac{1 + (\omega R_{ecl} C_0)^2}{1 + (\omega R_{ecl} C_t)^2} \times \frac{C_t}{C_0} \quad (3)$$

By choosing high frequency to which $\frac{1}{(\omega R_{ecl})}$ becomes sufficiently small compared with capacitance C in eq. (3) then it can be expressed as follows:

$$\tau X(t) = \frac{\frac{1}{(\omega R_{ecl})^2} + C_0^2}{\frac{1}{(\omega R_{ecl})^2} + C_t^2} \times \frac{C_t}{C_0} \cong \frac{C_0}{C_t} \quad (4)$$

The dielectric constants of C_0 and C_t are postulated to be ε_0 and ε_t, respectively. The electrode area is assumed to be S and the thickness of the cell layer is assumed to be d. Since the electrode area and thickness of the cell layer do not change with time, the following formula is obtained:

$$\tau X(t) = \frac{C_0}{C_t} = \frac{\varepsilon_0 \frac{S}{d}}{\varepsilon_t \frac{S}{d}} = \frac{\varepsilon_0}{\varepsilon_t} \quad (5)$$

From this formula, attention is paid to the change in the reactance component, and when the ratio of time course reactance is considered, $\tau X(t)$ expresses the ratio of the dielectric constant in the capacitance. Since the dielectric constant is a component of the capacitance of the cells, intraocular change is detected by $\tau X(t)$. In this experiment, $\tau X(t)$ decreased within 40 min after drug addition depending on drug density. From eq. (5), as ε_0 was not changed, the decrease in $\tau X(t)$ was caused by the increase in ε_t. An increase in the permittivity indicates a polarization gain in the dielectric substance. The substance noted in this experiment is the heme iron in the drug metabolism enzyme, and the redox reaction of the heme iron originates in the drug metabolism process. It is supposed that the heme iron which received the electron is easily polarized. As metabolic activity increases with the increase in the substrate concentration, the rate of heme iron which received the electrons in metabolic process will increase relatively. Consequently, the intracellular polarization ratio increases and dielectric constant also increases. It is expected that the polarization ratio can be detected in the increase in the dielectric constant.

CONCLUSION

In the present study it was indicated that the metabolic activity of the cells was able to be detected by the method of electrochemical impedance measurement. Moreover, the change in $\tau X(t)$ is not detected in the morphological change in the cell but in the enzyme intracellular activity. For this reason, this procedure be considered a revolutionary measuring method which can determine the metabolic activity of CYPs in the cells, so that the function of metabolism, which is closer to the organism, can be evaluated.

Acknowledgements

This work is supported financially by the NEDO project. I was informed of this by Professor T. Akaike of Tokyo Institute of Technology.

REFERENCES

1. Usui E, Noshiro M, Okuda K. Molecular cloning of cDNA for vitamin D3 25-hydroxylase from rat liver mitochondria. *FEBS Lett.* 1990; **262**(1): 135–138.

2. Nelson DR, Kamataki T, Waxman DJ, Guengerich FP, Estabrook RW, Feyereisen R, Gonzalez FJ, Coon MJ, Gunsalus IC, Gotoh O, Okuda K, Nebert DW. The P450 superfamily: update on new sequences, gene mapping, accession numbers, early trivial names of enzymes, and nomenclature. *DNA Cell Biol.* 1993; **12**(1): 1–51.
3. Okuda KI. Liver mitochondrial P450 involved in cholesterol catabolism and vitamin D activation. *J. Lipid Res.* 1994; **35**(3): 361–372.
4. Katagiri M, Ganguli BN, Gunsalus IC. A soluble cytochrome P-450 functional in methylene hydroxylation. *J. Biol. Chem.* 1968; **243**(12): 3543–3546.
5. Hedegaard J, Gunsalus IC. Mixed function oxidation. IV. An induced methylene hydroxylase in camphor oxidation. *J. Biol. Chem.* 1965; **240**(10): 4038–4043.
6. van 't Klooster GA, Woutersen-van Nijnanten FM, Blaauboer BJ, Noordhoek J, van Miert AS. Applicability of cultured hepatocytes derived from goat, sheep and cattle in comparative drug metabolism studies. *Xenobiotica* 1994; **24**(5): 417–428.
7. Matsusue K, Ariyoshi N, Oguri K, Koga N, Yoshimura H. Role of cytochrome b5 in the oxidative metabolism of polychlorinated biphenyls catalyzed by cytochrome P450. *Xenobiotica* 1996; **26**(4): 405–414.
8. Oritz de Montellano PR, Correia MA. Suicidal destruction of cytochrome P-450 during oxidative drug metabolism. *Annu. Rev. Pharmacol. Toxicol.* 1983; **23**: 481–503.
9. Bailey DG, Spence JD, Munoz C, Arnold JM. Interaction of citrus juices with felodipine and nifedipine. *Lancet* 1991; **337**(8736): 268–269.
10. White RE, Coon MJ. Oxygen activation by cytochrome P-450. *Annu. Rev. Biochem.* 1980; **49**: 315–356.
11. Sligar SG, Debrunner PG, Lipscomb JD, Namtvedt MJ, Gunsalus IC. A role of the putidaredoxin COOH-terminus in P-450cam (cytochrome m) hydroxylations. *Proc. Natl. Acad. Sci. USA* 1974; **71**(10): 3906–3910.
12. Sligar SG, Gunsalus IC. A thermodynamic model of regulation: modulation of redox equilibria in camphor monoxygenase. *Proc. Natl. Acad. Sci. USA* 1976; **73**(4): 1078–1082.
13. Sligar SG. Coupling of spin, substrate, and redox equilibriums in cytochrome P450. *Biochemistry* 1976; **15**(24): 5399–5406.
14. Transon C, Lecoeur S, Leemann T, Beaune P, Dayer P. Interindividual variability in catalytic activity and immunoreactivity of three major human liver cytochrome P450 isozymes. *Eur. J. Clin. Pharmacol.* 1996; **51**(1): 79–85.
15. Lee AJ, Kosh JW, Conney AH, Zhu BT. Characterization of the NADPH-dependent metabolism of 17beta-estradiol to multiple metabolites by human liver microsomes and selectively expressed human cytochrome P450 3A4 and 3A5. *J. Pharmacol. Exp. Ther.* 2001; **298**(2): 420–432.
16. Stresser DM, Blanchard AP, Turner SD, Erve JC, Dandeneau AA, Miller VP, Crespi CL. Substrate-dependent modulation of CYP3A4 catalytic activity: analysis of 27 test compounds with four fluorometric substrates. *Drug. Metab. Dispos.* 2000; **28**(12): 1440–1448.
17. Sugihara N, Ogoma Y, Abe K, Kondo Y, Akaike T. Immobilization of cytochrome P-450 and electrochemical control of its activity. *Polym. Adv. Technol.* 1998; **9**(5): 307–313.
18. Sugihara N, Ogoma Y, Abe K, Murakami Y, Kondo Y, Akaike T. Substrate specificity of camphor-induced cytochrome P-450 immobilized on an electrode. *Polym. Adv. Technol.* 1998; **9**(12): 858–860.
19. Sugihara N, Ogoma Y, Abe K, Murakami Y, Kondo Y, Akaike T. The relationship between the redox reaction of camphor-induced cytochrome P-450 and its activity. *Polym. Adv. Technol.* 1999; **10**(5): 265–269.
20. Modriansky M, Ulrichova J, Bachleda P, Anzenbacher P, Anzenbacherova E, Walterova D, Simanek V. Human hepatocyte-a model for toxicological studies. Functional and biochemical characterization. *Gen. Physiol. Biophys.* 2000; **19**(2): 223–235.
21. Hansen T, Borlak J, Bader A. Cytochrome P450 enzyme activity and protein expression in primary porcine enterocyte and hepatocyte cultures. *Xenobiotica* 2000; **30**(1): 27–46.
22. Rialland L, Guyomard C, Scotte M, Chesne C, Guillouzo A. Viability and drug metabolism capacity of alginate-entrapped hepatocytes after cryopreservation. *Cell Biol. Toxicol.* 2000; **16**(2): 105–116.
23. Omasa T, Kim K, Hiramatsu S, Katakura Y, Kishimoto M, Enosawa S, Suga K. Construction and evaluation for the liver functional HepG2 cell line in hybrid bioartificial liver support system. *Artificial Organs* 2001; **25**: 819.
24. Yoshida Y, Aoyama Y. Interaction of azole antifungal agents with cytochrome P-45014DM purified from Saccharomyces cerevisiae microsomes. *Biochem. Pharmacol.* 1987; **36**(2): 229–235.
25. Giaever I, Keese CR. Micromotion of mammalian cells measured electrically. *Proc. Natl. Acad. Sci. USA* 1991; **88**(17): 7896–7900.
26. Lo CM, Keese CR, Giaever I. Monitoring motion of confluent cells in tissue culture. *Exp. Cell Res.* 1993; **204**(1): 102–109.
27. Wegener J, Zink S, Rosen P, Galla H. Use of electrochemical impedance measurements to monitor beta-adrenergic stimulation of bovine aortic endothelial cells. *Pflugers Arch.* 1999; **437**(6): 925–934.
28. Lo CM, Keese CR, Giaever I. Impedance analysis of MDCK cells measured by electric cell-substrate impedance sensing. *Biophys. J.* 1995; **69**(6): 2800–2807.

Rapid Construction of gene-amplified CHO cell line by gene targeting

On-line Number 261

Takeshi Omasa[1], Mihoko Kajita[1], Tomohiro Yoshikawa[2], Yoshio Katakura[1], Michimasa Kishimoto[1] and Hisao Ohtake[1]

[1] Department of Biotechnology, Graduate School of Engineering, Osaka University, Yamadaoka 2-1 Suita Osaka 565-0871 Japan

[2] Research Institute for Cell Engineering (RICE), National Institute of Advanced Industrial Science and Technology(AIST), 3-11-46, Nakoji, Amagasaki, Hyogo, 661-0974 JAPAN

ABSTRACT

Gene amplification has been developed as an indispensable technique for the bio-pharmaceutical production by recombinant mammalian cells. The most commonly used technique is likely dihydroforate reductase (*dhfr*) gene amplification system in Chinese hamster ovary (CHO) cell line. In this gene amplification system, high productive CHO cells can be selected by "time-consuming" stepwise increases of methotrexiate (MTX) concentration in culture medium. However, it is of great significance to shorten the time for constructing the stable and productive recombinant CHO cell line in the industrial process. In this study, we focused on a rapid construction method for gene-amplified cell line. We employed the human granulocyte-macrophage colony stimulating factor (hGM-CSF) as a model of glycoprotein and investigated the relationship among the productivity and stability of amplified gene, the location of the amplified gene and the MTX concentration. The distribution of amplified gene on the chromosome was analyzed using fluorescence *in situ* hybridization (FISH). Based on the FISH image analysis, we speculated the specific chromosome location suitable for gene amplification.

KEY WORDS

gene amplification, chromosome targeting, CHO, fluorescence *in situ* hybridization

INTRODUCTION

Gene amplification is a widespread phenomenon in eukaryotes. It is an important process in the development of many organisms, emergence of drug resistance in tumor cells and some human parasites, and maturation of cancer cells. Furthermore, using cultured cells, the gene amplification phenomenon has been applied to the production of recombinant pharmaceuticals such as erythropoietin (EPO), granulocyte-colony-stimulating factor (G-CSF), and various antibodies (omasa, 2002). However, effective industrial process of recombinant protein production using mammalian cell lines has not been completely established because general methods for the construction of gene amplified cell lines have not yet been developed. Among those gene amplification techniques, the dihydrofolate reductase (*dhfr*) gene amplification system in the Chinese hamster ovary (CHO) cell line is the most widely used. For the application of a gene amplification system to industrial processes, one of the most important factors is the selection method employed for obtaining highly productive recombinant CHO cell lines that can stably produce desired recombinant proteins. However, the selection methods have so far been carried out only empirically and have been performed by trial and error. In this article, we analyzed the distribution of amplified gene on the chromosome using fluorescence *in situ* hybridization (FISH). Based on the FISH image analysis, we speculated the chromosome location suitable for gene amplification.

MATERIALS AND METHODS

The CHO DG44 cell line (dhfr$^-$), provided by Dr. L. Chasin of Columbia University, and was used as a host. The host cells were maintained in Iscove's modified DMEM (IMDM) (Sigma I-7633) with 10 % fetal bovine serum (FBS; Gibco), hypoxanthine (13.6 mg / L, Yamasa), and thymidine (2.42 mg / L, Yamasa). Transformants (dhfr$^+$; derived from DG44) were cultivated in a selection medium, IMDM with 10 % dialyzed FBS without hypoxanthine and thymidine. Cells were incubated under 5 % CO2 at 37 °C. For *dhfr* gene amplification, 10 to 1000 nM (final concentrations) of methotrexate (MTX) was added to the selection medium according to one of five patterns (Yoshikawa *et al.*, 2000a). We named these five heterogeneous cell pools DR1000L-1 to L-5. All these cell pools were obtained under a MTX concentration of 1000 nM. Using a limiting dilution assay, cell lines were cloned from these heterogeneous cell pools. In the limiting dilution assay, a cell suspension was diluted by IMDM medium to a concentration of one cell per 200 μL, and the diluted cell suspension was dispensed into a 96-well plate. These cloned cells were cultivated to a concentration of 10^6 cells per ml of medium. These selection steps were performed over one month.

The pSV2-dhfr/hGM-CSF vector was constructed from pSV2-dhfr (ATCC 37146) and pcD-hGM-CSF (ATCC 57594). The pSV2-dhfr vector contained mouse *dhfr* gene and the pcD-hGM-CSF vector

contained human GM-CSF gene. The promoter for both vectors was SV40 early promoter and the terminator was SV40-polyA. The details of the procedure for transfection were described previously (Yoshikawa *et al.*, 2000a,b).

Calculation of specific growth and hGM-CSF production rates

In order to evaluate the kinetic parameters for constructed cell pools and cell lines, we measured cell and hGM-CSF concentrations using batch cultures. Cell samples (1 vol.) were diluted with 0.16% trypan blue-0.85% NaCl solution, which stained only dead cells. The viable cell number was measured using a Bürker-Türk hemacytometer. This measurement method was described in detail by Omasa *et al.* (1992). The specific growth rate based on viable cells was calculated using the following equations (eqs. 1 and 2).

$$\frac{dXt}{dt} = \mu Xv \quad \text{.....eq. 1}$$

$$\ln(Xt) = \mu \int \left(\frac{Xv}{Xt} \right) dt + \ln(Xt)_0 \quad \text{.....eq. 2}$$

X_t and X_v are total and viable cell concentrations (cells / L), respectively. μ is specific growth rate (1 / h).t is cultivation time (h). The hGM-CSF concentration was measured by sandwich Enzyme-Linked Immunosorbent Assay (ELISA) using 96-well plates (Greiner 655061). The 96-well plate was previously coated over night at 4 °C with sheep anti-hGM-CSF antibody (580ng per well) (Endrogen P521). A 100 µl of culture supernatant was applied to each well and plates were incubated for 2 hr at 37 °C. Polyclonal rabbit anti-hGM-CSF antibody (Genzyme LP-714) was applied as the primary antibody (0.2µg per well) and plates were incubated for 2 hr at 37 °C. Alkaline phosphatase-conjugated anti-rabbit IgG antibody (Tago ALI3405) was used as the secondary antibody (0.1µg per well) and plates were incubated for 2 hr at 37 °C. After incubation, *p*-nitrophenyl phosphate (pNPP) (Sigma N-9389) was used as a substrate for alkaline phosphatase (0.2mg per well) and enzyme reaction was carried out for 1 hr at 37 °C. Purified recombinant hGM-CSF (Genzyme RH-CSF-C) was used as a standard. The absorbance of the sample was measured at 405 nm using an ELISA microplate reader (Tosoh MPR A4). The specific hGM-CSF production rate was calculated using the following equations (eqs. 3 and 4).

$$\frac{dP}{dt} = \rho Xv \quad \text{.....eq. 3}$$

$$P = \rho \int Xv dt + P_0 \quad \text{.....eq. 4}$$

P is hGM-CSF concentration in the medium (g /L) and ρ is specific human GM-CSF production rate

(g / cell / h). In order to evaluate the kinetic parameters of the constructed cell pools and lines, it is necessary to calculate the specific growth and human GM-CSF production rates with 95% confidential level based on Student's t distribution (Chatterjee *et al.*, 1991). As the results, the confidential level is less than 5% of specific rates. Therefore, the specific growth and human GM-CSF production rates were estimated by short batch cultures using the constructed cells (4 days).

Fluorescence in situ hybridization (FISH)

Chromosome spreads were prepared from exponential phase cultures using standard techniques (Carroll *et al.*1988). The cells were treated with colcemid (10 μg / ml) for 5 to 6 hr at 37 °C. The cells were suspended in a hypotonic solution (1.5 ml of 75 mM KCl) for 20 min at room temperature. After the hypotonic solution was decanted, freshly made fixative (3:1 Methanol / Acetic acids) was added. This procedure was repeated three times, and drops of the suspension were placed on a slide (Matsunami, S-2124) (Kuriki *et al.* 1993, Okumura, 1992). Fluorescence in situ hybridization (FISH) was performed as described by Pinkel *et al.* (1986). The details of FISH have been described previously (Yoshikawa *et al.* 2000). Based on the FISH image data, we constructed the ideogram using image analyzing system (Kato and Fukui 1998).

RESULTS AND DISCUSSION

We carried out stepwise increase in MTX concentration with five different selective conditions (pattern 1 to 5 in Figure 1). The specific growth (μ) and human GM-CSF production (ρ) rates in these cell pools were calculated at each stepwise increase in MTX concentration (Figure 1).

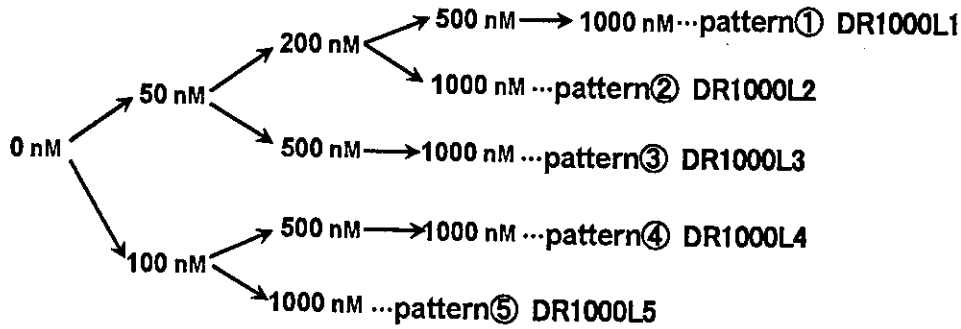

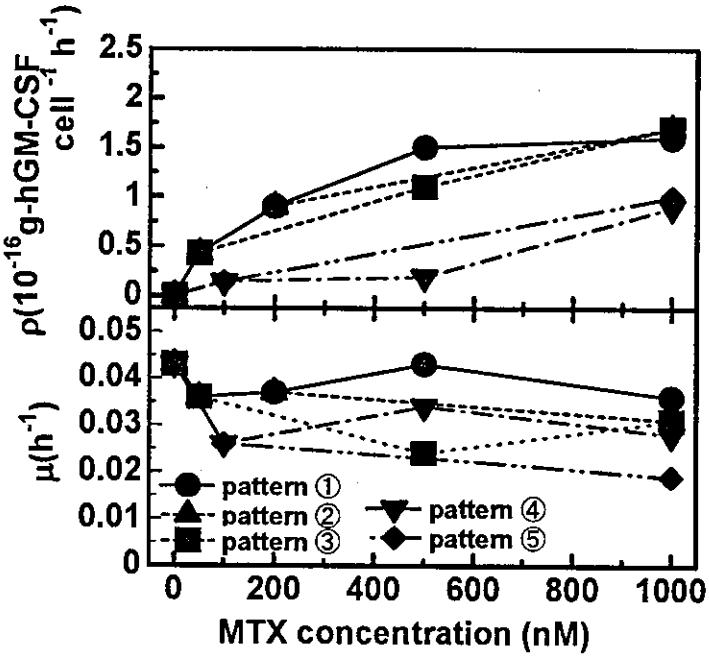

Figure 1 Relationship between patterns of increase in MTX concentration and specific growth and production rates and stepwise selection. The calculations of the specific growth rates are based on the use of heterogeneous cell pools.

The results revealed that the DR1000L1, L2 and L3 cell pools, cultivated in the presence of gradually increasing MTX concentrations, exhibited higher specific production rates than the other cell pools (DR1000L4 and L5). From these cell pools, we constructed cell lines for detail evaluation. The cell lines which had higher specific production rate were frequently obtained from the DR1000L1, L2 and L3 cell pools (Yoshikawa *et al.* 2000a). In the previous study, we classified the location of amplified genes into chromosomal DNA by observations (Yoshikawa *et al,* 2000a,b and 2001). In this study, we classified cell pools (DR1000L1 and L5) using image analysis. Figure 2 shows the ideogram patterns of DR1000L1 and L5 cell pools. We identified the twenty chromosomes in the amplified CHO cell. The amplified location was shown as a short bar. Each bar corresponds to the one observation of amplified gene.